Eduvest – Journal of Universal Studies
Volume 6 Number 8, August, 2026
p- ISSN 2775-3735- e-ISSN 2775-3727

Numerical Study of the Effect of Notches on Main Cooling Water Pump Shaft Failure

Muhammad Firda Fattahuddian*, Achmad Syaifudin
Institut Teknologi Sepuluh Nopember, Indonesia
Email: firda.fattahuddian@plnindonesiapower.co.id*, syaifudin@its.ac.id

Keywords
Fatigue Failure, Main Cooling Water Pump, Finite Element Analysis, Peterson Chart, Partial-Arc Geometry

ABSTRACT
The Main Cooling Water Pump (MCWP) is critical in geothermal plants, since failure reduces capacity and increases downtime. This study investigates the fatigue failure of an ASTM A276 Type 316 stainless-steel MCWP shaft at an Indonesian geothermal plant, fractured by a grinding notch from overhaul. The unresolved problem is that the notch was identified only visually, without quantitative stress-concentration, fatigue-life, or numerical validation for repair-radius decisions. A Palmgren–Miner cumulative-damage analysis across startup, steady-state, and shutdown phases shows the baseline notch (r = 0.735 mm; Kts = 3.98) yields Dtotal = 0.6338 at 720 days, while D = 1 requires r ≈ 0.634–0.655 mm, only 14% sharper than baseline. ANSYS Mechanical 2025 R2 simulations across five repair radii (r = 4, 6, 8, 10, 11 mm) revealed a U-shaped Peterson-chart-versus-FEA deviation from a partial-arc effect: since repair depth is limited to 3 mm, the transition-arc fraction drops from 100% at baseline to 48.1% at the largest radius. The novelty of this study is characterizing this partial-arc mechanism quantitatively, distinct from the r/d-based chart deviations reported in prior work. For maintenance and asset management, stress reduction increases with radius up to r = 11 mm, while r = 6 mm marks the smallest chart-to-FEA deviation, which grows again at larger radii; a 0.1 mm radius change shifts damage from 63% to 100% of life, precise enough to guide repair-radius and inspection intervals. By quantifying this partial-arc limit on chart reliability, the study gives maintenance engineers a defensible, data-driven basis for repair-radius selection.

INTRODUCTION

The Main Cooling Water Pump (MCWP) is a critical auxiliary component in geothermal power plants: its failure can significantly reduce generating capacity and increase maintenance downtime, since removing the pump requires large-capacity lifting equipment. At the geothermal power plant studied here, the MCWP Unit 3 shaft experienced a fatigue failure on September 12, 2022, identified during a pump inspection triggered by a loss of discharge pressure and abnormal motor current following restart.

The failure of the Main Cooling Water Pump (MCWP) shaft Unit 3 of the study plant was found on the upper side of the impeller during the pump dismantling process (Haryanto et al., 2024; Khan et al., 2026; Riddell, 2026; Sondar et al., 2021; Whittaker et al., 2023). A similar problem has been reported by Hamid (2018) on the shaft of the Circulating Water Pump

(CWP) made of Austenitic Stainless-Steel type 316, which reported that the shaft material exhibited porosity and that fatigue cracking initiated from the outer surface, with hardness testing indicating a brittle pearlite microstructure at the fracture region. However, the study has not examined the effect of the loading cycle during the start, operation, and shutdown phases on the fatigue life of the shaft or provided recommendations for changes in the geometry of the fault area. In the case of the MCWP of the study plant, the 2020 internal inspection report identified the presence of grinding wounds or notches on the shaft surface as the main cause of shaft fractures. However, these conclusions are only based on visual observations without the support of quantitative analysis of the magnitude of voltage concentration, fatigue life, or validation through numerical simulations, so they cannot be used as a strong scientific basis in determining similar failure repair and prevention strategies.

This pattern is not unique to the study plant. Notch-driven fatigue is recognized as the dominant failure mode across rotating machinery worldwide, spanning power generation, mining, and transportation (Hou et al., 2022), with comparable cases reported for pump and shaft-bearing failures in Brazil (de Lacerda et al., 2024), China (Guo et al., 2021), and elsewhere (Hua et al., 2023), reinforcing the broader engineering relevance of the notch-radius sensitivity analysis undertaken here. Despite this recognition, a specific gap remains in how repair-radius selection is technically justified: chart-based methods such as the Peterson chart, and the FEA validation studies that have tested their accuracy (Sivák et al., 2023), assume an enlarged notch radius forms a complete transition arc, whereas in-situ shaft repairs are frequently constrained by a maximum allowable material-removal depth. To the authors' knowledge, no prior study has examined how this depth constraint affects chart-based Kt/Kf reliability, or distinguished this partial-arc condition from the general r/d-based deviation already documented in the literature.

The novelty of this study is twofold: it back-calculates, via Palmgren–Miner cumulative damage, the notch radius mathematically required to explain the shaft's actual 720-day failure duration, and it quantifies the partial-arc mechanism itself, showing that Peterson-chart Kt/Kf reliability depends not only on r/d, as previously reported, but also on how much of the idealized transition arc is actually achieved under a fixed repair depth. This yields two complementary contributions: theoretically, the study extends Peterson-chart-based Kt/Kf estimation by introducing arc fraction as a second geometric variable alongside r/d; practically, it gives plant engineers a quantitative, defensible basis, in place of the purely visual assessment used previously, for selecting repair radii and setting inspection intervals.

Based on these conditions, this study is directed at two objectives. The first objective is to determine the equivalent notch radius and stress concentration factor (Kts) at the grinding notch using the Peterson chart, together with the notch radius mathematically required to match the observed 720-day failure duration through a Palmgren–Miner back-calculation. The second objective is to determine the deviation in stress concentration factor (Kt) and fatigue factor (Kf) between the Peterson chart and Finite Element Analysis (FEA) simulation across a series of repair radii, including how the limited depth of an in-situ repair produces a partial-arc transition geometry that affects the reliability of the Peterson chart's prediction. The analysis is focused on an MCWP shaft made of ASTM A276 Type 316 under the torsional loading that occurs during the startup, stable operation, and shutdown phases, evaluated across a baseline notch geometry and a series of repair radii so that the partial-arc effect on Peterson-chart reliability can be characterized quantitatively.

Quantitative fatigue-life and damage assessment of this kind is broadly essential wherever structural or rotating components are subjected to cyclic or dynamic loading, since undetected fatigue damage can compromise structural integrity across many classes of load-bearing equipment (Suprianto et al., 2023; Izzuddin et al., 2025).

The resulting characterization of notch-radius sensitivity and partial-arc effects is intended as a quantitative basis for repair-radius selection and preventive inspection planning on similar MCWP units.

METHODS

Research Flow

This study analyzed the failure of the MCWP shaft made of ASTM A276 Type 316. The research begins with collection of shaft geometry data (including the grinding notch dimensions) and pump operating load data across the startup, steady-state, and shutdown conditions. The shaft and its supporting components are then modeled in ANSYS Mechanical 2025 R2 and validated against the actual geometric conditions of the shaft in the fatigue-fracture area, so that the equivalent notch radius and stress concentration factors obtained analytically and numerically can be compared consistently across the baseline and repair-radius geometries.

Data and Analytical Basis

Motor and pump specification data (power, torque, starting current, and torque–speed curves) were obtained from the manufacturer's operation and maintenance manual (Ansaldo, 1997) and combined with in-plant measurements. The S–N curve was constructed using the Basquin equation with cyclic material parameters for AISI 316 from Chou et al. (2016), whose chemical composition is identical to the ASTM A276 316 shaft material, with the effective endurance limit corrected via the Marine equation for surface condition, size, load type, temperature, and reliability.

Load histories for the three governing phases startup (breakdown-torque transient, obtained through Euler-method numerical integration of the equation of rotational motion at 5% speed intervals), steady-state operation (from EWS current-log data, 24 November–1 December 2025), and shutdown/trip were each converted to torque and nominal stress on the shaft.

The stress concentration factor at the grinding notch was obtained from the Peterson chart, with a notch-sensitivity correction applied to determine the effective torsional Kf. Since the exact grinding-wheel fillet radius could not be measured directly, the lower-bound radius achievable with the 101.6 mm (4 in), 1.2 mm-thick wheel used in the 2020 overhaul ($r = 0.735$ mm, $r/d = 0.005$) was adopted as the baseline, coinciding with the chart's lower validity limit and the sharpest credible geometry consistent with the fracture.

Cycle counting for the Palmgren–Miner damage summation followed the Simple-Range Counting method per ASTM E1049-85 (2017), chosen because the operating load history is periodic with known turning points and, for loading without nested loops, yields results identical to Rainflow Counting.

ANSYS

Modeling was carried out in ANSYS 2025 R2 following a three-stage workflow pre-processing, processing, and post-processing applied consistently across the baseline geometry and the five repair-radius geometries.

Pre-processing. The shaft geometry the baseline grinding-notch profile and, for the repair cases, the notch re-modeled as a smooth concave arc (r = 4, 6, 8, 10, and 11 mm) was built and modified in ANSYS SpaceClaim, then assigned the material properties of ASTM A276 Type 316. The critical zone (the notch/transition-arc region, cross-sectional changes, and bearing-support area) was discretized with quadratic 10-node tetrahedral elements (Tet10) at a locally refined element size, ranging from 0.050 mm at the sharp baseline notch to 0.748 mm at the largest repair radius, to resolve the steep local stress gradient without making the full-model solve computationally prohibitive. Mesh adequacy was verified through an elements-per-180°-arc density count (46.2 elements/180°, exceeding the 16-elements/180° threshold recommended by Leitner et al., 2017).

A skewness check on the final Tet10 mesh gave minimum 1.305×10^{-10}, maximum 0.99792, mean 0.23135, and standard deviation 0.12419; the mean falls within the **Very Good** category according to the ANSYS criterion of < 0.25, as shown in the mesh quality distribution histogram (Figure 1).

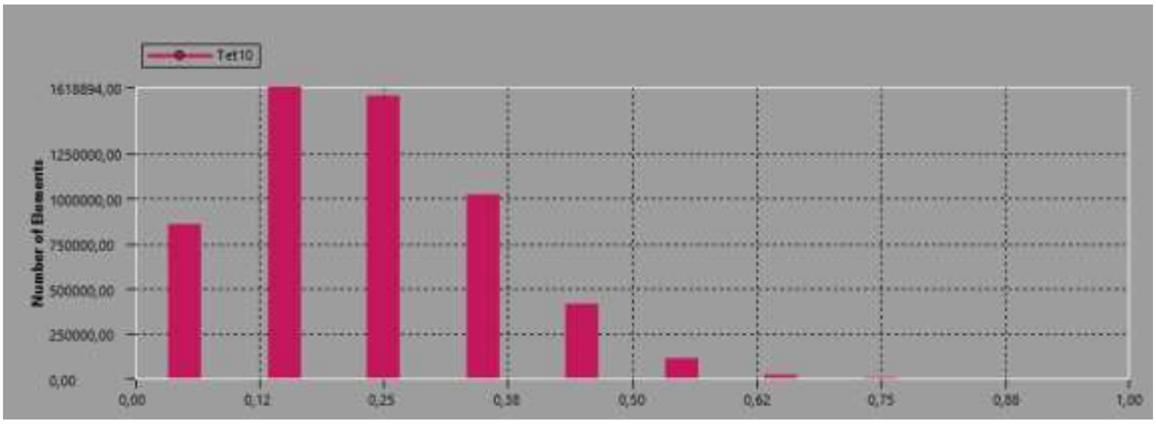

Figure 1 skewness histogram

Beyond this density criterion, a mesh-convergence (h-refinement) sensitivity study at the baseline notch, spanning six element sizes from 0.10 to 0.03 mm, showed the stepwise change in notch-root stress falling from 2.95% to 0.57%, reaching $\Delta S = 1.22\%$ at the adopted 0.05 mm size (46.2 elements/180°). This exceeds both the grid-convergence framework of Roache (1994) and an independent mesh-density benchmark for notch-fatigue assessment (12–16 elements/180°) reported by Braun et al. (2020), whose parameter study found under-resolved notch meshes can produce fatigue-life errors of up to 185%. This sweep constitutes the sensitivity analysis performed on the FEA model itself.

Processing. Boundary conditions followed the physical configuration of a vertical pump: the thrust-bearing location was modeled as a fixed support, since it carries the entire axial load of the shaft, while the rubber bearing was modeled as a remote displacement that constrains radial motion but allows rotation, consistent with its role as a guide bearing. The torque obtained from the load calculations was applied as a moment at the driven end, and each of the six geometric models (baseline and five repair radii) was solved as an independent static structural analysis under the governing startup breakdown-torque condition.

Post-processing. For each solved model, the equivalent (von Mises) stress and the maximum principal stress were extracted at the notch/transition-arc root, together with the corresponding FEA-based stress concentration factor $K_{t,FEA} = \sigma_{VM,max}/\sigma_{nom}$. These results (Table 1) were then compared against the Peterson-chart predictions at the same r/d ratios to quantify the analytical–numerical deviation and the partial-arc effect examined in the following sections. Lacking experimental or field measurement (see Results), model credibility instead relies on the mesh-convergence benchmarking above and consistency with Peterson-chart predictions within its validated range.

Model Assumptions. The FEA model assumes: (i) linear-elastic material behavior; (ii) single-step static-structural solution at peak startup breakdown-torque load; (iii) fixed support at the thrust bearing and remote displacement at the guide bearing, rather than explicit bearing stiffness; (iv) homogeneous ASTM A276 Type 316 with no residual stress, corrosion, or pre-existing crack; and (v) no nonlinear contact, so each model solves directly.

Several limitations should be acknowledged. First, the baseline notch radius (r = 0.735 mm) is a chart-based reading rather than a direct metrological measurement, so the back-calculated range (r ≈ 0.634–0.655 mm) should be read as a sensitivity estimate, not an as-built dimension. Second, all FEA models are static-structural and linear-elastic, evaluated at peak startup load only. Third, mesh-independence was verified only at the baseline geometry; the same density criterion was then applied, rather than re-verified, at each repair radius, so a residual discretization uncertainty cannot be excluded there. Fourth, the notch-sensitivity factor differs by case: the baseline uses q = 0.631 (at r = 0.735 mm), while the five repair radii use a single q ≈ 0.817 (evaluated at an intermediate radius via the Neuber–Abarkan relation) held constant rather than recalculated at each radius, an effect largest at the extremes of that range. These limitations do not change the qualitative findings the notch-radius sensitivity of fatigue life and the partial-arc deviation pattern but they bound the quantitative precision of the specific Kts, Kf, and D_{total} values reported, and they motivate the direct metrological and experimental validation recommended in the Conclusion.

RESULT AND DISCUSSION

Stress Concentration and Fatigue Regime Analysis

Analytical calculation of the notch-affected cross-section shows that the equivalent stress at the grinding notch reaches σ_{eq} = 268.82 MPa (Kts = 3.98, Kf = 2.880, r/d = 0.005), which exceeds the material yield strength (Sy = 241 MPa). This places the startup breakdown-torque phase in the Low Cycle Fatigue (LCF) regime, while the steady-state operation and shutdown phases remain elastic. This stress state indicates that the failure is driven primarily by torsional stress concentration at the grinding notch rather than by the loading itself, since the shaft geometry and operating torque alone, without the notch, would remain within the High Cycle Fatigue regime. The adequacy of this notch-based explanation for the observed failure timing is examined quantitatively in the back-calculation analysis below.

Back-calculation of the Required Notch Radius

To verify whether the notch geometry read from the Peterson chart (Kts = 3.98, r = 0.735 mm, r/d = 0.005) is sufficient to explain the actual failure duration of the shaft (720 days), a

Palmgren–Miner cumulative-damage analysis was performed for a pure-torsion loading scenario, combining the startup breakdown-torque phase, steady-state operation, and shutdown/trip. Using the cyclic material parameters of AISI 316 (equivalent to ASTM A276 316) from Chou et al. (2016), the resulting cumulative damage is D_total = 0.6338 at 720 days below the Miner failure threshold (D = 1) with the steady-state operation phase contributing 99.2% of the total damage due to its very large cycle count relative to the startup phase.

Because Kts = 3.98 does not by itself account for the observed failure duration, a back-calculation was carried out to determine the notch radius that would be required to reach D_total = 1 within 720 days. Solving for the required stress concentration factor gives Kts, required = 4.148. Substituting this value into the Peterson torsion formula, $Kts = 1.953 + 0.1434x - 0.0021x^2$ ($x = 0.1/(r/d)$), yields two mathematical roots; selecting the root consistent with the physical trend of the curve gives r ≈ 0.634 mm. This result was cross-checked with an independent power-law fit of the same Kts–r data ($Kts = 3.605 \cdot r^{-0.326}$), which gives a consistent estimate of r ≈ 0.650 mm.

Both estimates (r ≈ 0.634–0.655 mm) are smaller than the smallest radius supported by the validated range of the Peterson chart used (r/d ≥ 0.005, i.e. r ≥ 0.735 mm for this shaft diameter). This indicates that the actual notch geometry is likely sharper than the smallest radius the chart was validated for, so the resulting values should be treated as a sensitivity estimate rather than a direct, chart-validated reading. This finding motivates the use of Finite Element Analysis, which is not bound by the r/d range of the analytical chart, as an independent validation method, and is discussed further in the following section together with the effect of partial-arc geometry on the repair radii.

FEA Stress Results Across a Series of Repair Radii (r = 4, 6, 8, 10, 11 mm)

To evaluate the effect of enlarging the notch radius, the geometric discontinuity at the grinding notch is converted into a smooth transition profile with a radius of R = 11 mm along the 300 mm critical zone. This principle is based on the basic concept of fatigue mechanics that the voltage gradient at the root notch is inversely proportional to the root radius the larger the r, the smaller the local voltage amplification (Pilkey, Bi & Pilkey, 2020).

The value r = 11 mm was established based on Peterson's chart readings for the Keyway shaft Location B (fillet) from Pilkey, Bi & Pilkey (2020). At r/d = 11/147 = 0.075, the Kt,Peterson value of the Location B graph was read as 2.1 with a notch sensitivity factor of 1.8. sensitive to changes in radius geometry.

1. ANSYS Mechanical 2025 R2 Simulation Results

Table 1 ANSYS simulation results σ_VM.max various repair radii (mesh equivalent to 46.2 elements/180°)

r (mm)	σ_VM,max (MPa)	S1,max (MPa)	Kt,FEA	Element size (mm)
0,735 (baseline)	231,87	130,37	2,484	0,050
4	186,63	143,62	2,000	0,272
6	181,55	123,25	1,944	0,408
8	164,55	94,618	1,763	0,544
10	153,15	88,315	1,641	0,680
11	131,00	80,44	1,403	0,748

Table 1 summarizes the raw FEA output for the baseline and all five repair radii. Two trends are apparent. First, σ_VM,max decreases monotonically with radius, from 231.87 MPa at baseline to 131.00 MPa at r = 11 mm, consistent with the contour pattern in Figure 2. Second, Kt,FEA also decreases monotonically, from 2.484 at baseline to 1.403 at r = 11 mm; this Kt,FEA column is the FEA-side value used for every comparison against the Peterson-chart Kts in the deviation analysis that follows. The element size column reflects the mesh refinement applied at each notch geometry (0.050–0.748 mm) to keep the minimum-elements-per-180° criterion satisfied as the transition radius enlarges.

Figure 2 Von Mises stress distribution across the five repair-radius models (unified legend, 2.78–191.4 MPa)

Figure 2 presents the von Mises stress contours of all five repair-radius models on a single unified color-scale legend (2.78–191.4 MPa), so that the stress intensity can be compared visually and directly across radii rather than relying on five separately auto-scaled plots. The red-orange band at the notch root is widest and most intense at r = 4 mm, then visibly narrows and shifts toward green-yellow as the radius increases through r = 6, 8, and 10 mm, and is smallest at r = 11 mm, where the contour along the transition arc stays mostly in the green range. This visual trend is consistent with the numerical σ_VM,max values already presented in Table 1, confirming that the stress reduction visible here is not an artifact of per-model color scaling.

It should be noted that all stress values reported above are numerical (analytical and FEA) results; no strain-gauge measurement, photoelastic test, or physical fatigue test was performed on the actual shaft or on a scaled specimen to experimentally validate σ_VM,max or Kt,FEA, since the shaft is an operating company asset and destructive or intrusive testing of this kind was not available within the scope of the present study. The FEA model itself was validated indirectly, through mesh-quality checks (Section 3.3) and through consistency with the Peterson-chart trend at r/d ratios within the chart's validated range, rather than through direct physical measurement. This absence of experimental validation is a limitation of the present results and is why direct metrological and experimental confirmation is recommended as follow-up work in the Conclusion.

2. Analytical vs ANSYS Deviation and Justification

The deviation between σanalytic and σVM, ANSYS is calculated using

Deviation (%) = (σ_analitik − σ_VM,FEA) / σ_analitik × 100%

Table 2 Analytical Kts/Kf (Peterson) and Deviation from FEA Results, Baseline and Repair Radii

r (mm)	R/D	Kts Peterson	Kf	p_analitik (MPa)	σ_VM,ANSYS (MPa)	Deviation
0,735	0,0050	3,980	2,880	268,82	231,87	+13,75%
4	0,0272	2,452	2,186	204,04	186,63	+8,53%
6	0,0408	2,292	2,055	191,85	181,55	+5,37%
8	0,0544	2,209	1,988	185,57	164,55	+11,33%
10	0,0680	2,159	1,947	181,75	153,15	+15,73%
11	0,0748	2,141	1,932	180,34	131,00	+27,36%

This 13.75% deviation is reasonable and consistent with the literature because:

a. σ_analitik uses Kf which already includes a material sensitivity correction ($q = 0.817$), whereas ANSYS generates a voltage from a purely elastic geometry so that it reflects Kt,FEA;
b. Kt,FEA < Kf because ANSYS models full 3D voltage redistribution whereas Peterson's Kf is conservative 2D [Pilkey, Bi & Pilkey, 2020];
c. $r/d = 0.005$ lies below the smallest ratio actually tested by Sivák et al. (2023) ($r/d \geq 0.01$), so the baseline case falls outside the range their comparison covers; within their tested range, for the $D/d \approx 1.01$ band closest to a single-diameter shaft they report a Kt deviation of about −13% to −7%, consistent with the deviation magnitude observed here.

A deviation of 13.75% at baseline ($r/d = 0.005$) validates the ANSYS model and confirms that there is a systematic difference between the Peterson-chart stress-concentration estimate, which is conservative, and the FEA result, which reflects the actual stress state on the shaft.

The results of the FEA simulation show that enlarging the notch radius from baseline ($r = 0.735$ mm) across the repair radius range ($r = 4$–11 mm) provides a significant reduction in stress concentration. With a mesh equivalent of 46.2 elements/180° across the entire model, the maximum von Mises stress decreases monotonically as the radius increases: from 231.87 MPa (baseline) to 186.63 MPa ($r = 4$ mm) to 131.00 MPa ($r = 11$ mm). This monotonic stress-reduction trend provides the Kt,FEA values used in the deviation analysis below.

Comparison of the Peterson Chart and FEA: Effect of Partial-Arc Geometry

Table 2 shows that the deviation between Kts,Peterson and Kt,FEA does not vary monotonically with r/d; instead it forms a U-shaped pattern, decreasing from the sharp baseline notch toward a minimum at intermediate radii and then increasing again at the largest repair radius. This pattern cannot be explained by radius alone and is examined here in terms of the arc geometry actually formed during the repair.

The Peterson chart used in this study (for a keyway shaft without a key) is built from a single independent variable, the radius-to-diameter ratio (r/d), under the structural assumption that the radius r always forms a full 90° transition arc from the base of the notch to a tangential connection with the shaft surface. Because the material-removal depth in an in-situ repair is limited (in this case to a maximum of 3 mm, to preserve the shaft's dimensional integrity), the actual arc angle θ formed by a given radius r follows the geometric relation

$$\text{depth} = r \times (1 - \cos \theta)$$

so that the maximum arc angle achievable at a limited removal depth is $\theta = \arccos(1 - 3/r)$, capped at 90°. Because the Peterson chart has no mechanism to accept θ as an input separate from r/d, it always returns the same Kts value for a given r/d, regardless of how much of the 90° arc is physically achieved.

Table 3 lists the depth required to form a full 90° arc at each repair radius, the depth actually available (3 mm), the resulting actual arc angle, and the corresponding arc fraction (θ/90°). At the baseline notch (r = 0.735 mm), the available depth is more than sufficient, so the arc fraction is effectively 100%; the large deviation observed at this radius is instead attributable to the chart's reduced accuracy at the lower edge of its validated range, consistent with Sivák et al. (2023). From r = 4 mm upward, the fixed 3 mm removal depth becomes insufficient to form a full arc, and the arc fraction falls steadily to 48.1% at r = 11 mm.

Table 3 Actual Arc Angle vs. Repair Radius

r (mm)	Depth needed for 90° (mm)	Depth available (mm)	Actual θ (°)	Arc fraction θ/90° (%)
0.735	0.735	3	90.0	100
4	4	3	75.5	83.9
6	6	3	60.0	66.7
8	8	3	51.3	57.0
10	10	3	45.6	50.6
11	11	3	43.3	48.1

This partial-arc effect explains why Kt,FEA declines more steeply than Kts,Peterson at larger radii: because the material-removal depth is fixed, the transition becomes progressively less than a full 90° arc as r increases, which effectively softens the notch beyond what the chart assumes. The Peterson chart, receiving only r/d as input, cannot detect this and continues to report Kts as if a full arc were formed, so the gap between the chart estimate and the FEA result widens again at the largest radii even though the physical notch is objectively smoother.

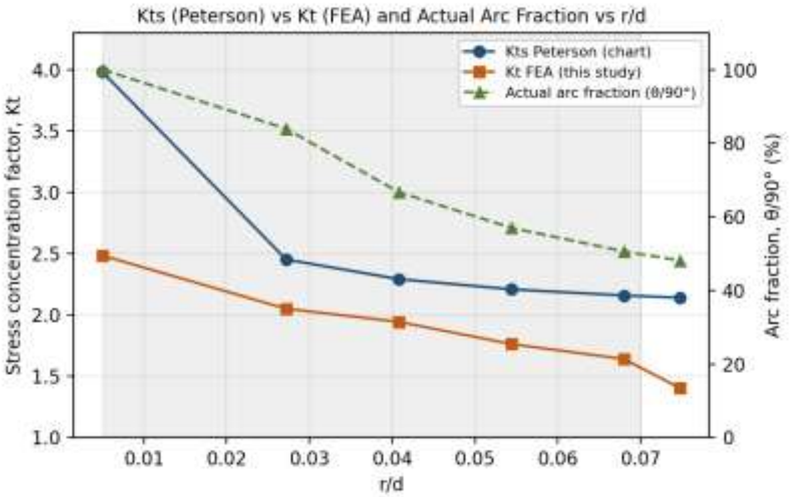

Figure 3 Kts (Peterson) and Kt (FEA) together with the actual arc fraction (θ/90°) versus r/d

Because the chart provides no way to distinguish a full arc from a partial one, using it directly for repair-radius selection in cases with a limited material-removal depth can produce a Kts value that departs substantially from the actual repaired geometry, particularly at larger radii where the achieved arc fraction is farthest from 100%. This is consistent with the wider finding of Sivák et al. (2023), who report that analytical/FEM deviations for notch stress-concentration factors are not one-directional but depend on the specific combination of geometric ratios involved; a single chart lookup should therefore be treated as a conservative first estimate rather than a substitute for FEA validation whenever the repaired geometry departs from the chart's idealized full-arc assumption. This limitation reinforces the role of FEA established in the back-calculation analysis above: because the chart's validated range ($0.005 \le r/d \le 0.07$) also cannot represent partial-arc geometry, FEA is required as an independent check for repair radii both within and beyond that range.

To place these results in the context of independent literature, Table 4 compares the deviation of Kf (Peterson vs. FEA, corrected for notch sensitivity via the Neuber relation) obtained in this study with the ΔαTi deviation reported by Sivák et al. (2023) for a keyseat-type geometry at the nearest comparable diameter ratio in their dataset, D/d ≈ 1.01 (the geometric configuration closest to a single-diameter shaft such as the one studied here).

Table 4 Comparison of Kf Deviation (This Study) with Sivák et al. (2023) ΔαTi at D/d ≈ 1.01

r (mm)	r/d	Kf Peterson	Kf FEA	Deviation Kf (%)	Arc fraction (%)	ΔαTi Sivák (D/d≈1.01) (%)
0.735	0.0050	2.880	1.936	−32.8	100	−13.5
4	0.0272	2.186	1.840	−15.8	83.9	−10
6	0.0408	2.055	1.784	−13.2	66.7	−8.5
8	0.0544	1.988	1.648	−17.1	57.0	−8
10	0.0680	1.947	1.553	−20.2	50.6	−7.5
11	0.0748	1.932	1.350	−30.1	48.1	−7

Both datasets show the analytical estimate deviating from the FEA/FEM result in the same direction (i.e., the chart-based Kf and αTi values do not match the numerical result), but the magnitude in this study is larger, particularly at the baseline (−32.8% vs. −13.5%) and at the largest repair radius (−30.1% vs. −7%). Sivák et al. (2023) worked with fillet geometries under tensile loading and a two-diameter shaft (D/d), whereas this study involves a keyseat-type notch under torsion on a single-diameter shaft; the larger deviation observed here is consistent with the partial-arc effect discussed above, which has no counterpart in Sivák et al.'s configuration. Sivák et al. (2023) explicitly report that the sign and magnitude of chart-to-FEM deviation depend on the specific combination of geometric ratios (r/d and D/d) rather than following one consistent direction; because the MCWP shaft has no D/d parameter to vary, this study cannot verify whether the deviation direction found here would reverse under a different geometric combination, so the comparison is presented as an independent directional check rather than a validation of matching magnitudes.

Beyond the stress-concentration comparison, these results connect to the physical mechanism of notch-driven fatigue. Shaft failures across mechanical equipment are dominated by notches and fillets, where the local stress gradient drives crack nucleation before the nominal section is at risk (Hou et al., 2022); the notch root radius controls not only peak stress (Kt) but the stress distribution relevant to subsequent fracture-mechanics analysis (Braun et al., 2022), consistent with the 2020 inspection finding that the grinding notch, not bulk defects, caused the fracture.

The U-shaped deviation in Table 4 has a data-grounded explanation rather than reflecting scatter. At the baseline (r/d = 0.0050), the geometry sits at the chart's lower validity boundary ($0.005 \le r/d \le 0.07$). At r = 11 mm (r/d = 0.0748), the geometry falls just outside the chart's upper boundary, and the achievable arc has fallen to 48.1% of a full 90° fillet (Table 3), violating the chart's full-arc assumption. Only near r = 6 mm (r/d = 0.0408, arc fraction 66.7%) do both conditions hold well enough for chart and FEA to agree closely   though, as discussed below, this is a reliability optimum, not a stress optimum, since peak stress itself decreases monotonically with radius (Table 1). A comparable trend, that notch sharpness rather than depth governs fatigue life, has been reported for notched AISI 316L specimens, where V-notch profiles produced markedly shorter fatigue lives than rounded or rectangular notches of comparable depth (Jatavallabhula et al., 2026). Physical confirmation of this crack-initiation mechanism for the MCWP shaft through fractographic examination of the failed surface was outside the scope of the present study and is recommended as a direct extension of this work.

Not every chart-versus-FEA comparison in the literature finds deviations of this magnitude. For a shoulder fillet in torsion (r/d = 0.052) and a keyway fillet (r/d = 0.0208), both well inside the chart's validated range with gentle transition geometries, Peterson's chart, FEA, and independent photoelastic data (Fessler et al., 1969, as cited in Jordaan, 2025) showed excellent mutual agreement (Jordaan, 2025). The present study's largest deviations instead occur at the two extremes of the r/d range examined, where the chart's validity or full-arc assumption is violated. Read together, these studies suggest chart-to-FEA agreement depends on where the geometry sits relative to the chart's validated range, not on a fixed property of the method; the good agreement reported for gentle, mid-range fillets should not be extrapolated to sharp notches or depth-constrained repairs of the kind examined here.

For maintenance planning, this stress-reduction-versus-chart-deviation trade-off (r = 11 mm for maximum stress reduction, r = 6 mm for the smallest chart-to-FEA gap, a consequence of arc fraction still being comparatively high there) should be weighed explicitly rather than assuming one radius is best on both counts (quantified in the Conclusion). Separately, the sensitivity of fatigue life to notch radius has direct inspection-planning implications: a radius reduction of only about 0.1 mm, from 0.735 mm to the back-calculated 0.634 mm, is enough to shift the cumulative damage at 720 days from D = 0.6338 to the failure threshold D = 1.0, a 58% increase for that small a change in geometry so inspection intervals for similar MCWP shafts should incorporate a margin beyond the nominal 720-day baseline.

Limitations

Several limitations bound these conclusions, beyond those already noted in Methods: the FEA model does not capture sub-second startup transients; the baseline notch radius is a chart-based estimate rather than a direct measurement; mesh-independence was verified only at the baseline geometry; and q was held constant across repair radii. Most significantly, no experimental or field measurement (strain gauge, photoelastic test, or fractographic examination) was performed, since the shaft is an operating company asset and destructive testing was not available within this study's scope; the FEA model was instead benchmarked indirectly, through mesh-convergence criteria and Peterson-chart consistency (Methods). None of these change the qualitative findings, but they bound the precision of the values reported and motivate the follow-up recommended in the Conclusion.

CONCLUSION

This study shows the MCWP shaft's fatigue failure was caused by a grinding notch, shifting the startup breakdown-torque phase to Low Cycle Fatigue (σ_{eq} = 268.82 MPa > S_y = 241 MPa); steady-state and shutdown stayed elastic. A Palmgren–Miner back-calculation showed the chart-read radius (K_{ts} = 3.98, r = 0.735 mm) cannot alone explain the 720-day failure; the required radius (r ≈ 0.634–0.655 mm) is outside the chart's range. Comparing the chart and FEA across repair radii (r = 4–11 mm) revealed a U-shaped deviation from a partial-arc effect: since repair depth was limited to 3 mm, the chart's full-arc assumption could not represent the declining arc fraction (100% to 48.1%), diverging again at the largest radii, absent from Sivák et al.'s (2023) validation study, whose broader finding is directionally consistent. Repair-radius selection involves a trade-off: r = 11 mm gives the greatest stress reduction (231.87 to 131.00 MPa, ~43%), while r = 6 mm gives the smallest chart-to-FEA deviation (−13.2%, nontrivial); both should be weighed explicitly. A 0.1 mm radius change shifts cumulative damage from D = 0.6338 to the failure threshold D = 1.0 (a 58% increase), so inspection intervals should not rely on the 720-day baseline alone. FEA, not the chart alone, should guide repair-radius selection whenever field repairs must preserve shaft dimensions and minimize material removal, constraints that limit achievable depth and produce the partial, sub-90° arc the chart cannot represent; metrological measurement should confirm the radius; and overhaul should use stricter workmanship.

REFERENCES

Braun, M., Fischer, C., Baumgartner, J., Hecht, M., & Varfolomeev, I. (2022). Fatigue crack initiation and propagation relation of notched specimens with welded joint characteristics. *Metals, 12*(4), 615.

Braun, M., Müller, A. M., Milaković, A. S., Fricke, W., & Ehlers, S. (2020). Requirements for stress gradient-based fatigue assessment of notched structures according to theory of critical distance. *Fatigue & Fracture of Engineering Materials & Structures, 43*(7), 1541–1554.

Chou, L.-H., Chiou, Y.-C., Wu, C.-C., & Huang, Y.-J. (2016). Predictions of stress-strain curve and fatigue life for AISI 316 stainless steel in cyclic straining. *Journal of Marine Science and Technology, 24*(3).

de Lacerda, J. C., Teixeira, R. L. P., dos Reis, W. D., Garcia, A. S. T., de Brito, T. G., & Brito, R. F. (2024). Fracture analysis of a centrifugal ore slurry pump shaft: A study using fatigue tests, microstructural analysis and finite element simulation. *Multiscale and Multidisciplinary Modeling, Experiments and Design, 8*, 83.

Guo, H., Duan, H., Lei, J., Wang, D., Du, S., Zhang, Y., & Ding, Z. (2021). Failure analysis of automobile engine pump shaft bearing. *Advances in Mechanical Engineering, 13*(4).

Hamid, A., Nugroho, S., Haryadi, G. D., & Khaeroman. (2018). Failure analysis of shaft circulating water pump (CWP) used in power plant. *MATEC Web of Conferences, 159*, 02027.

Haryanto, M., Andryansyah, A., Amelia, A. C., & Parikin, P. (2024). Failure analysis on a cooling water pump of the power plants. *AIP Conference Proceedings, 2967*(1), 100005.

Hou, N., Ding, N., Qu, S., Guo, W., Liu, L., Xu, N., Tian, L., Xu, H., Chen, X., Zaïri, F., & Wu, C. M. (2022). Failure modes, mechanisms and causes of shafts in mechanical equipment. *Engineering Failure Analysis, 136*, 106216.

Hua, M., Cao, C., Cai, Y., Ge, J., Zhong, F., & Mao, J. (2023). Failure analysis and structural fatigue resistance design of multistage centrifugal pump shaft. *Engineering Failure Analysis, 153*.

Izzuddin, M. Y., Syaifudin, A., Rahmat, M. F., & Suwarmin. (2025). Finite element-based fatigue analysis of medium-speed train car structure. *International Review of Mechanical Engineering, 19*(9), 472–483.

Jatavallabhula, J. K., Gundeti, S. R., Pavan Kumar, D., Ananda Kumar, L. M., & Venkata Satyanarayana, V. (2026). Finite element-assisted fatigue life evaluation of notched AISI 316L: Comparative insights into V-notch and rectangular notch geometries. *EPJ Web of Conferences, 345*, 01013.

Jordaan, J. P. (2025). Case study: Evaluation of stress concentration factors in shaft keyways through FE analysis. *R&D Journal, 41*, 1–8.

Khan, R., Ahmad, M., Ali, S., Qahtani, F., Talha, T., Alqaed, S., Mustafa, J., & Safdar, S. O. (2026). Failure analysis of a centrifugal pump impeller in erosive flow conditions. *Engineering Failure Analysis*, 110584.

Leitner, M., Pauer, P., Kainzinger, P., & Eichlseder, W. (2017). Numerical effects on notch fatigue strength assessment of non-welded and welded components. *Computers & Structures, 191*, 51–61.

Neuber, H. (1961). *Theory of notch stresses: Principles for exact stress calculation*. U.S. Office of Technical Services.

Pilkey, W. D., Pilkey, D. F., & Bi, Z. (2020). *Peterson's stress concentration factors* (4th ed.). John Wiley & Sons.

Riddell, R. (2026). *Centrifugal pump reliability 101: Practical solutions through fundamentals and case studies*. CRC Press.

Roache, P. J. (1994). Perspective: A method for uniform reporting of grid refinement studies. *Journal of Fluids Engineering, 116*(3), 405–413.

Sivák, P., Delyová, I., & Bocko, J. (2023). Comparison of stress concentration factors obtained by different methods. *Applied Sciences, 13*(24), 13328.

Sondar, P. R., Kumar, J. K. R., Chawla, S., Dsilva, P. C., & Hegde, S. R. (2021). Failure of a cooling water pump shaft. *Journal of Failure Analysis and Prevention, 21*(1), 149–159.

Suprianto, T., Syaifudin, A., Pamungkas, L. W., Ariatedja, J. B., & Farid, A. R. (2023). Effect of fluctuating load on fatigue of PPCW flat wagon. *The International Journal of Mechanical Engineering and Sciences, 7*(1), 26–35.

Whittaker, S., Sidhu, S., & Subramanian, M. (2023). Case study on catastrophic failure of the cooling water pump DE bearing. *Abu Dhabi International Petroleum Exhibition and Conference*, D021S057R004.